Proc. 18th Conf. Planned and Inadvertent Weath. Mod., Seattle, WA, 24-27 Jan.; AMS, Boston, MA

J15.2 CCN Effects on Simulated Storm Electrification and Precipitation

Edward Mansell*[1] and Conrad L. Ziegler[1]

1. INTRODUCTION

The effects of the concentration of cloud condensation nuclei (CCN) on cloud microphysics have long been recognized, although the impact of CCN on the precipitation and electrification processes in convective storms has been relatively unexplored. In the present study, the impact of varying CCN concentration on the microphysics and electrification of a small multicell storm is simulated with a 3-dimensional cloud model. Previous studies on CCN effects on electrification using explicit charging parameterizations has been limited to axisymmetric (Takahashi 1984) and 1D (Mitzeva et al. 2006) models. Furthermore, these two studies only tested two values of CCN concentration, so no trends could be studied. Electrification is highly sensitive to graupel production and collisions between graupel and smaller ice particles. CCN aerosol effects are suspected to play a significant role in differences in lightning production between maritime and continental thunderstorms.

The effects of the concentration of cloud condensation nuclei (CCN) on cloud microphysics have long been recognized (e.g., Pruppacher and Klett 1978). The potential impact of CCN on the precipitation process in convective storms is of great interest, since microphysics, and precipitation formation in particular, may strongly impact several areas of storm analysis and forecasting: for example, airflow dynamics, hydrology, electrification, chemistry, and their numerical predictions.

Precipitation in convective storms develops via some combination of warm- and cold-cloud processes. The warm-cloud process is dominated by the combined effects of condensation with quasi-stochastic drop coalescence (i.e., binary coalescence or "self-collection" of cloud droplets to form drizzle-sized rain drops, followed by rain collection of cloud and rain "self-collection"). The cold-cloud process is initiated mainly by production of graupel embryos via: (1) drop freezing; and (2) vapor nucleation of crystals followed by riming of vapor-grown and aggregated snow particles. Subsequent precipitation growth is dominated by graupel riming of cloud. Rain is predominantly produced from graupel meltwater.

*Corresponding author address: Dr. Edward Mansell, National Severe Storms Laboratory (NSSL), 120 David L. Boren Blvd, Norman, OK 73072
[1]NOAA/NSSL, Norman, Oklahoma

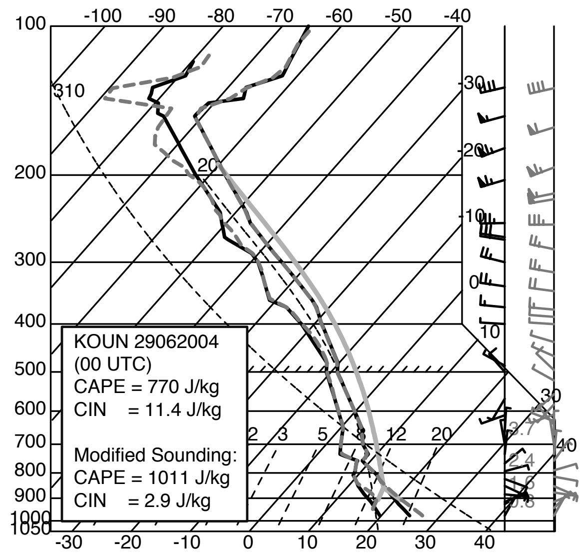

Figure 1: Original and modified soundings.

The CCN concentration has the capacity to modulate the warm- and cold-cloud processes in several ways. For example, low (or alternatively, high) CCN forces the nucleation of low (high) concentrations of large (small) droplets, which in turn increase (decrease) the coalescence rate and accelerate (slow) the growth of rain drops. Graupel develop high (low) bulk densities and fallspeeds via riming of large (small) droplets. Frozen-drop graupel embryo formation is regulated by the median volume size of coalesced drops (which in turn is CCN-dependent) at temperatures at or colder than about -5 to -10 °C.

The impact of CCN on convective storm evolution has been examined using numerical cloud models. For example, Li et al. (2008) implemented a two-moment bulk microphysics scheme in the WRF model, finding that precipitation in a simulated Texas Gulf coast storm increases with increasing CCN concentration from low to moderately high values due to suppression of warm rain coalescence and enhancement of the mixed phase precipitation process. Van Den Heever and Cotton (2007) demonstrated that simulated storm dynamics was sensitive to suppression of the warm rain process caused by CCN enhancement, thereby exerting a strong influence on precipitation by effectively modulating the time-integrated updraft vapor supply.

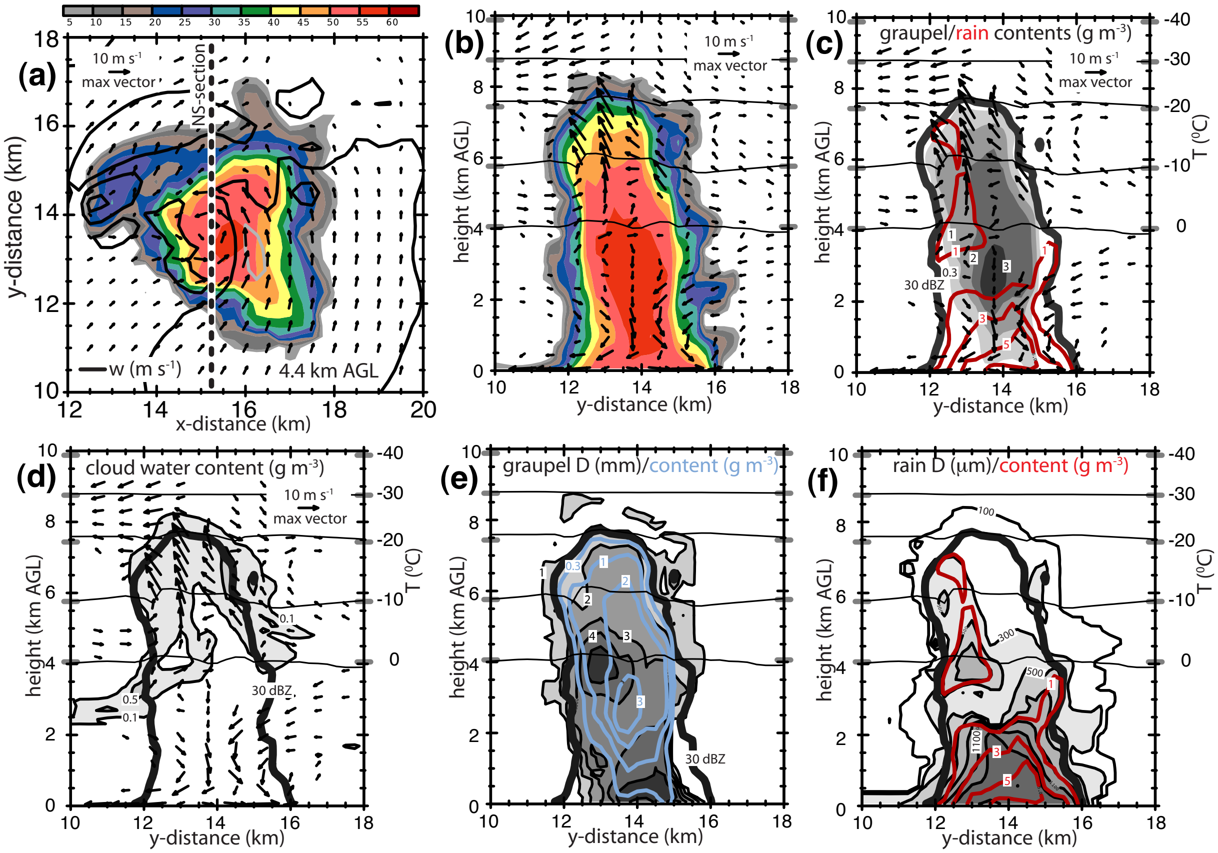

Figure 2: Cross-section at 51 min of the simulation using CCN concentration of 500 cm^{-3}. (a) Horizontal section of reflectivity with horizontal wind vectors and contours of vertical velocity (contour interval of 3 m s^{-1}). Panels (b-f) depict quantities in a S-N cross-section [indicated on (a)]. The heavy black contour in (c-f) is the 30 dBZ reflectivity outline. (b) Reflectivity and wind vectors. (c) Graupel content (0.3, 1, 2, 3 g m^{-3}) in gray-filled contours and rain content (1, 3, 5 g m^{-3}) in red. (d) Cloud water content (0.1, 0.5 g m^{-3}). (e) Graupel mean volume diameter (1 to 5 mm by 1 mm, gray filled) and graupel content as in (c). (f) Rain mean volume diameter (300 to 1500 μm by 200 μm, gray filled) and rain content as in (c).

In the present study, the impact of varying CCN concentration of the parent airmass on the subsequent microphysical structure and lightning production of a small, multicell storm is explored with a high-resolution, three-dimensional cloud model.

2. CLOUD MODEL

a. Airflow dynamics

This study uses the Collaborative Model for Multiscale Atmospheric Simulation (COMMAS) (Wicker and Wilhelmson 1995). As described in Coniglio et al. (2006), the model uses the basic equation set from Klemp and Wilhelmson (1978) and prognostic equations are included for momentum, pressure, potential temperature, and turbulent kinetic energy (Deardorff 1980). Time integration is performed either with a third-order Runge--Kutta (RK) scheme (Wicker and Skamarock 2002) or a forward-in-time scheme. Advection on the first two RK iterations uses 5th-order upwind differencing. On the final RK step, certain scalar quantities (potential temperature and vapor mixing ratio) and wind components are advected with a 5th-order weighted essentially non-oscillatory (WENO) scheme (Jiang and Shu 1996; Shu 2003). All other scalars (e.g., mixing ratio, number concentration) are advected with a forward-in-time 6th-order Crowley scheme (Tremback et al. 1987) with a 1-D monotonic limiter (Leonard, 1991). Sedimentation uses a first-order upwind scheme, with corrections for the two-moment variables as in Mansell (2010) to prevent spurious large particles and radar reflectivities.

b. Microphysics

The cloud model employs a two/three-moment (bulk) microphysical parameterization scheme which describes form and phase changes among a range of

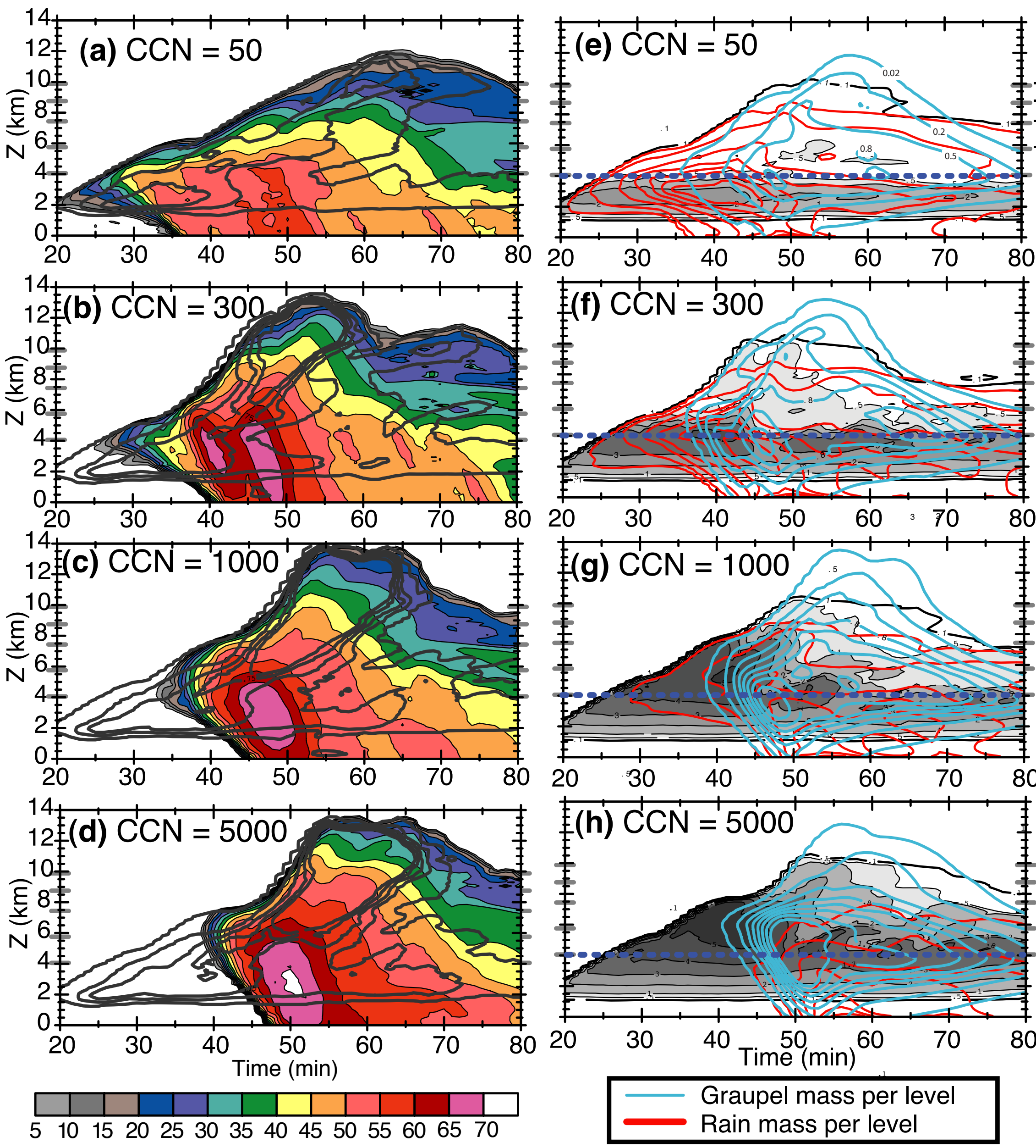

Figure 3: (a-d) Time-height maximum simulated radar reflectivity (color contours) and updraft volume (w > 5 m/s; black contours at 0.01, 0.25, 0.5. 0.75, 1 km^3 per level). (e-h) Time-height maximum cloud water content (gray shading), and horizontally integrated rain (red contours) and graupel (blue contours) masses. In (f-j), the horizontal dashed line is the environmental 0C level. Contour levels in (e-h) for graupel mass are 0.02 and >= 0.2 x 10^6kg by intervals of 0.3, and for rain mass are 0.02, 0.2, and >= 1 x 10^6kg by intervals of 1.

liquid and ice hydrometeors (Mansell et al. 2010). The microphysical parameterization predicts the mass mixing ratio and number concentration of cloud droplets, rain drops, cloud ice crystals, pristine and aggregated snow crystals, graupel, and hail. Graupel and hail can be three-moment variables with prediction of the 6th moment in diameter (proportional to radar reflectivity). In the present study, graupel was 3-moment, and the hail category was turned off. Additionally, the liquid water fraction on snow and graupel is predicted following Ferrier (1994), and graupel particle density is predicted (Mansell et al. 2010).

Hydrometeor size distributions are assumed to follow a self-preserving Gamma functional form. Transfer rates between the vapor phase and the various hydrometeor categories are derived from governing equations for individual particles integrated over the appropriate hydrometeor size distribution. Microphysical processes include cloud droplet and cloud ice nucleation, condensation/deposition, evaporation/sublimation, collection-coalescence, variable density riming, shedding, ice multiplication, cloud ice aggregation, freezing and melting, and conversions between hydrometeor categories. CCN concentration is predicted as a single-category, bulk spectrum ($N_o S^k$, where k=0.6) approximating small aerosols. In the rest of this paper, N_o is equivalent to CCN concentration, which also places a limit on droplet activation. That is, the local CCN concentration is depleted as droplets are activated.

The cloud model predicts the bulk graupel and hail particle densities as functions of rime layer density. Rime density in turn is a function of droplet size (e.g., affected by CCN concentration), impact speed, and ambient temperature. The graupel and hail particle densities are also used as roughness parameters to scale the drag coefficient in the expressions for particle fall speed.

The prediction of hydrometeor number concentration (and therefore charge separation) is particularly critical to the resolution of secondary ice nucleation at higher temperatures (-5 < T < -20 C) in the mixed phase updraft region, where ice crystals may be produced both by rime fracturing (Hallett–Mossop process) and by splintering of freezing drops in addition to a range of primary nucleation mechanisms.

c. Electrification and Lightning

Electrification parameterizations follow Mansell et al. (2005, 2010), including noninductive charge transfer between graupel particles and ice/snow particles, inductive charging between graupel and small droplets, and small ion processes (e.g., generation by cosmic rays, recombination, attachment to hydrometeors, drift, and corona point discharge at the ground). For this study, noninductive charging is based on the laboratory results of Saunders and Peck (1998). In the present set of experiments, total inductive charge separation is overall generally an order of magnitude weaker than total noninductive charging.

Lighting discharges are simulated with a stochastic 3D branched parameterization (Mansell et al. 2002). Breakdown is initiated when the electric field magnitude exceeds a height-dependent threshold (see Mansell et al. 2010). Lightning channels are treated as imperfect conductors, and the charge induced on the channels is released as small ions.

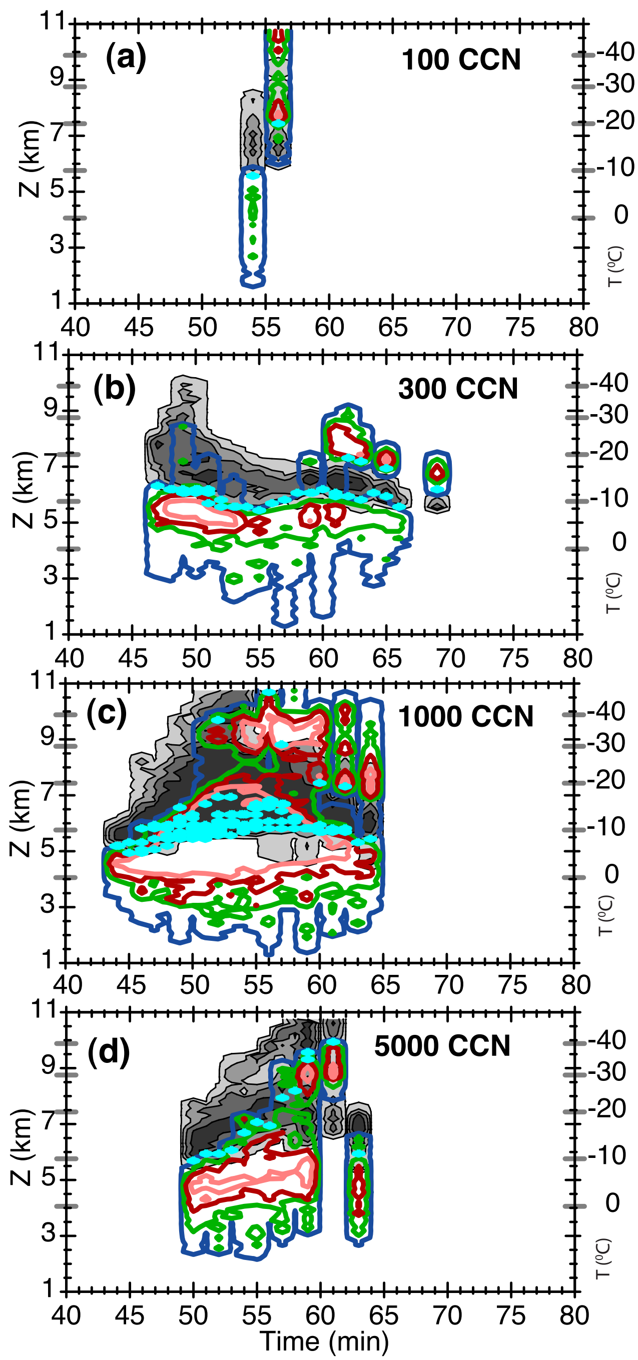

Figure 4: Time-height lightning channel segments and initiation points. Lightning channels are summed by model level. Positively-charged channels are shown in gray-filled contours, while colored contours indicate channels that carried negative charge. The cyan diamonds show times and heights of lightning initiation. The lightning activity reflects the gross charge structure of the storm.

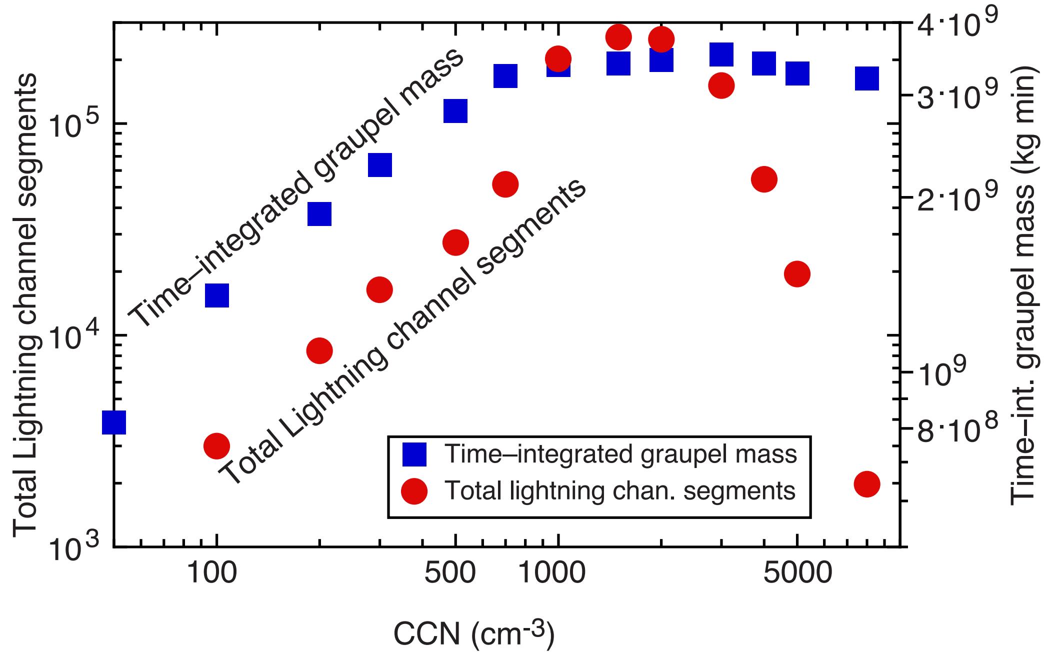

Figure 5: Time-integrated graupel mass and lightning segments (proportional to total channel length) for all 13 simulations (CCN from 50 to 8000 cm^{-3}). No lightning occurred for CCN

The lightning ions can then attach to hydrometeors and diffuse to neighboring grid points.

d. Model domain, initialization, and integration

The horizontally-homogeneous model environment was initialized from the 00 UTC 29 June National Weather Service operational sounding (Fig. 1). Sounding modifications reduced the mixed layer convective inhibition (CIN) from 11.4 to 2.9 J kg^{-1} and increased CAPE from about 770 to 1011 J kg^{-1}. Simulations were performed in a 30-km by 30-km by 21.6-km domain with constant grid spacing of 250 m in the horizontal and 125 m in the vertical from the surface to 10 km, above which the grid spacing was gradually stretched to a maximum of 500 m. The time step was 4 sec.

Vertical motion was initiated by applying a constant acceleration term to vertical velocity in the boundary layer. The updraft nudging method introduces deep moist convection more smoothly than the conventional thermal bubble initialization and is also more representative of roll-type mesoscale updraft forcing of convection initiation (e.g., Ziegler et al. 1997). Details of the updraft forcing term and random thermal perturbations can be found in Mansell et al. (2010).

A set of 13 simulations was run using the same initial conditions (and forcing) except for the base value of CCN concentration, which varied from 50 to 8000 cm^{-3}. Initial CCN concentrations are assumed to be vertically well-mixed, and are therefore scaled by air density as $CCN(z) = CCN_{base} [\rho_{air}(z)/\rho_o]$. In other words, the CCN number mixing ratio (number per kg of dry air) is assumed constant in the domain.

3. RESULTS, DISCUSSION AND CONCLUSIONS

a. Mature storm morphology

The model case with CCN = 500 cm^{-3} (similar to the control run of Mansell et al. 2010) illustrates the typical structure of the mature simulated storm near the time of peak overall precipitation and updraft intensity (Fig. 2). The initial updraft core in the storm, centered at approximately (x,y) = (15 km, 14.5 km) at higher levels (not shown), is decaying at 51 min, while a newer updraft core is developing on the west flank of the main precipitation core (Fig. 2a). In a vertical south-to-north cross-section (Fig. 2b), the main precipitation core is downdraft-dominated below and updraft- dominated above 0°C. Mixed-phase conditions combining graupel (Fig. 2c,e) with rain drops (Fig. 2c,f) and supercooled cloud droplets (Fig. 2d) increasingly characterize the sub-freezing updraft core region by around 51 min.

b. Bulk storm evolution with differing CCN

Model sensitivity tests with a range of ambient CCN concentrations (50 to 8000 cm^{-3}) control the mean droplet size at cloud base, thereby modulating drop growth via condensation-coalescence in environments effectively ranging from clean

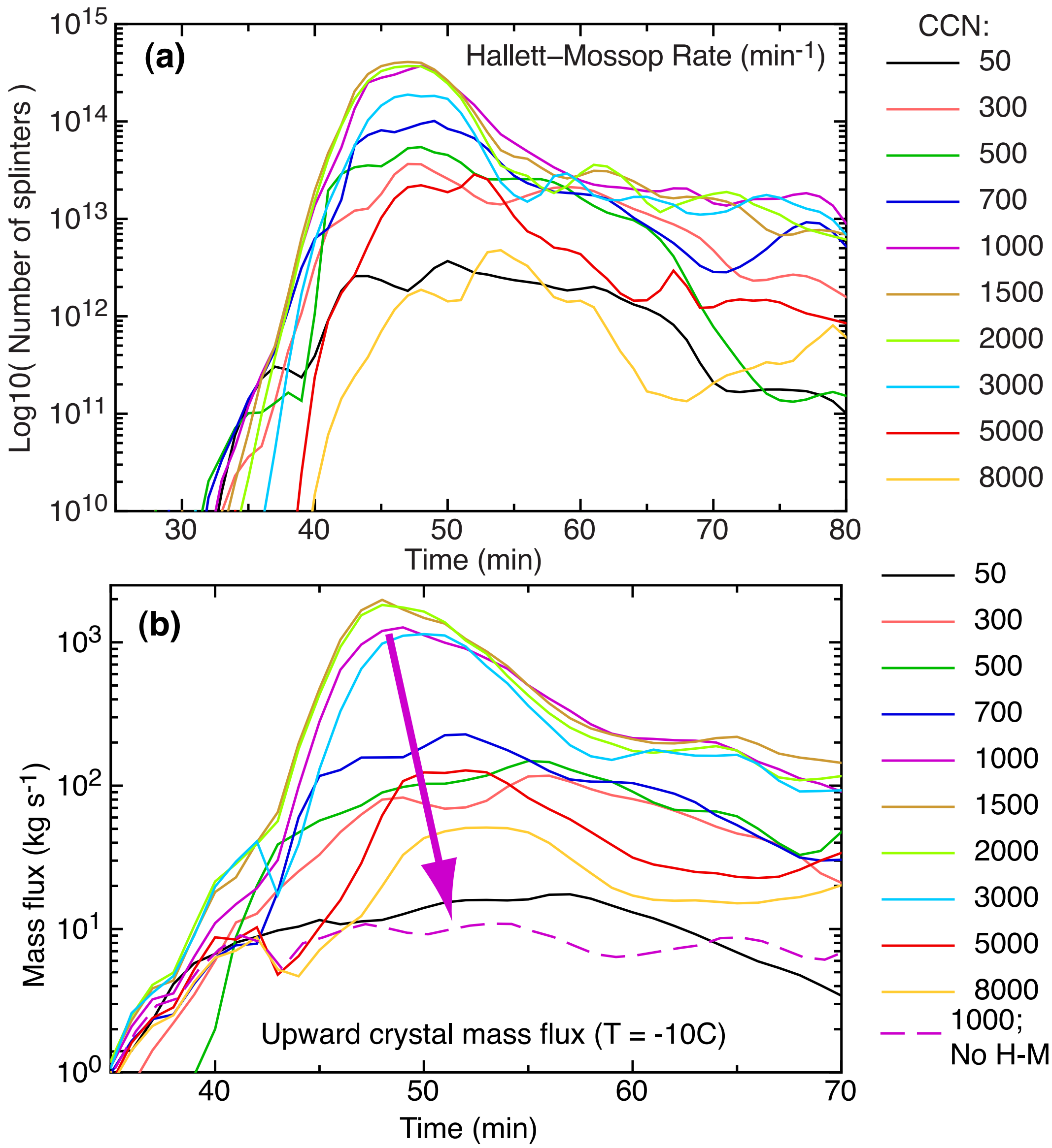

Figure 6: Time-series of (a) ice multiplication rate (Hallett-Mossop process) and (b) upward ice crystal mass flux through the -10°C level. The arrow in (b) connects the 1000 cm^{-3} curves with (solid) and without (dashed) ice multiplication.

maritime to extreme continental (Fig 3). The simulated time-height reflectivity, graupel mass, rain mass, and updraft volume all show systematic variations in their evolutions as base CCN concentration increases.

Precipitation in the simulated storm first initiates as raindrops via stochastic collision-coalescence in regions of high cloud water content. Higher CCN concentrations reduce the collision-coalescence formation of rain/drizzle, which also shifts the initial reflectivity echoes to later times and higher altitudes (Fig. 3a-d). Raindrops lifted in updraft begin freezing at temperatures around -10°C to form graupel. Precipitation mass gradually becomes dominated by graupel-based, cold-cloud riming process relative to the warm rain process (Fig. 3e-h).

As higher CCN concentrations cause increasing delay times for rain formation, drops appear at higher altitudes (lower temperature) (Fig. 3e-h) and have less time to accrete droplets before freezing. Even at the highest CCN concentrations, rain/drizzle appeared before graupel, because the vapor supply in the updraft remained sufficient for droplets to eventually grow large enough via condensation to accelerate drop coalescence growth. The warm-cloud depth restricted primary ice crystal initiation to higher altitudes in the cloud, such that drop freezing

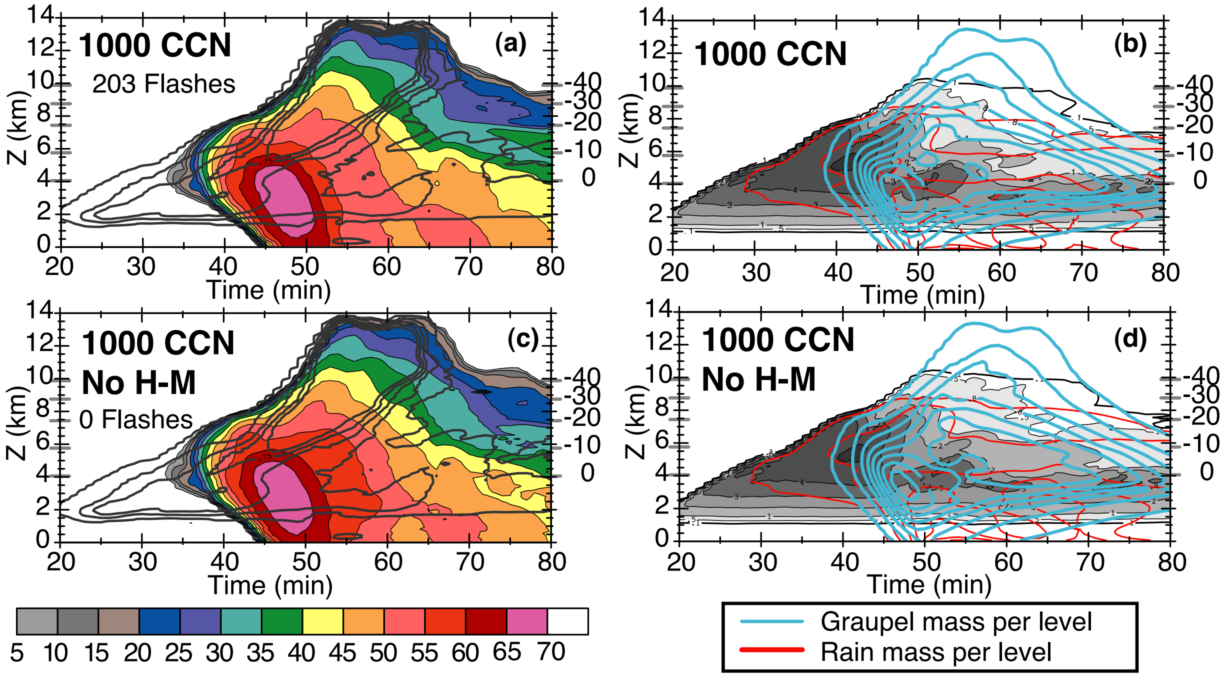

Figure 7: As in Fig. 3 for CCN concentration of 1000 cm^{-3}, comparing with and without secondary ice multiplication (Hallett-Mossop process). (a-b) Repeat of Fig. 3c,g with activated secondary ice. (c-d) Same as (a-b) but secondary ice process deactivated.

appeared to the primary source of initial graupel in this case.

c. Effects on electrification and lightning activity

Without question, the significant effects of CCN concentration on storm microphysical structure should thereby affect electrification. The increases in graupel mass seen in Fig. 3e-g did indeed appear to result in increased lightning activity (Fig. 4). Lightning activity decreased, however, as CCN concentration was increased from 1000 to 5000 cm^{-3} (Fig. 4c-d) whereas graupel did not appreciably decrease (Fig. 3g-h).

An overall upward trend in both total graupel and lightning segments (i.e., channel length) is seen as CCN concentration was increased from 50 to 1000 cm^{-3} (Fig 5). (Channel length convolves frequency and extent of lightning flashes and is used here as a measure of lightning activity.) As CCN concentration was further increased, total graupel saw little change whereas lightning channel length dropped sharply, with only one lightning flash for CCN of 8000 cm^{-3}.

Since graupel mass remains steady for CCN concentrations greater than about 1000 cm^{-3}, one might suspect that the other ingredient for noninductive charging is responsible, i.e., smaller ice particles (cloud ice and snow). As shown in Fig. 6b, the upward ice crystal mass flux through the -10°C level increased dramatically as CCN increased from 50 to 1000 cm^{-3}, and then started to decrease again at 2000 cm^{-3} and higher. The primary source of this increase and decrease is the secondary ice multiplication process (Fig. 6a, Hallett-Mossop). The initial increase in ice multiplication is a factor of increased graupel production and subsequent riming. The decrease at high CCN concentration is a consequence of the dependence of parameterization of the Hallett-Mossop on the existence of cloud droplets with diameters greater than 24 microns. At extremely high CCN values, the large concentrations of droplets sufficiently restricts the bulk condensational growth of their mean diameter such that the number of larger droplets is greatly reduced. The combination of enhanced ice multiplication and subsequent vapor-depositional growth provides large ice crystals for efficient noninductive charging (Ziegler et al. 1991).

An additional test was run with CCN concentration of 1000 cm^{-3} but Hallett-Mossop turned off. The arrow in Fig. 6b shows the dramatic drop in upward ice crystal mass flux. The electrification without Hallett-Mossop was similar to the 50 cm^{-3} case: significant electrification but insufficient electric field magnitude for lighting initiation. The deactivation of the Hallett-Mossop parameterization has negligible effect on the storm evolution (Fig. 7), so the drastic change in electrification via ice crystal reduction is wholly an effect on ice-ice collision rates and not a change in storm intensity in any way.

To summarize, the effects of CCN concentration on electrification are highly dependent on parameterizations of microphysical processes. These effects may be unexpected. For the range of expected CCN concentrations (up to about 2000 cm^{-3}), the model simulations suggest monotonic increases in graupel and lightning production. A smaller set of tests with more a intense storm (higher CAPE environment, not shown) suggests a similar trend using the same set of model parameterizations.

4. ACKNOWLEDGEMENTS

Support was provided by the National Severe Storms Laboratory. Partial funding for this research was provided by NSF grant ATM-0451639. Some of the computing for this project was performed at the OU Supercomputing Center for Education & Research (OSCER) at the University of Oklahoma (OU).

5. REFERENCES

Coniglio, M. C., D. J. Stensrud, and L. J. Wicker, 2006: Effects of upper-level shear on the structure and maintenance of strong quasi-linear mesoscale convective systems. J. Atmos. Sci., 63, 1231–1252.

Deardorff, J. W., 1980: Stratocumulus-capped mixed layers derived from a three-dimensional model. Bound.-Layer Meteor., 18, 495–527.

Ferrier, B. S., 1994: A double-moment multiple-phase four-class bulk ice scheme. Part I: Description. *J. Atmos. Sci.*, **51**, 249–280.

Jiang, G.-S. and C.-W. Shu, 1996: Efficient implementation of weighted ENO schemes. J. Comp. Phys., 126, 202–228.

Klemp, J. B. and R. B. Wilhelmson, 1978: The simulations of three-dimensional convective storm dynamics. J. Atmos. Sci., 35, 1070–1096.

Leonard, B. P., 1991: The ULTIMATE conservative difference scheme applied to unsteady one-dimensional advection. Comput. Methods Appl. Mech. Eng., 88, 17–74.

Mansell, E. R., D. R. MacGorman, C. L. Ziegler, and J. M. Straka, 2002: Simulated three-dimensional branched lightning in a numerical thunderstorm model. *J. Geophys. Res.*, **107**, doi: 10.1029/2000JD000244.

Mansell, E. R., D. R. MacGorman, C. L. Ziegler, and J. M. Straka, 2005: Charge structure and lightning sensitivity in a simulated multicell thunderstorm. *J. Geophys. Res.*, **110**, doi:10.1029/2004JD005287.

Mansell, E. R., C. L. Ziegler, and E. C. Bruning, 2010, Simulated electrification of a small thunderstorm with two-moment bulk microphysics. J. Atmos. Sci., 67, 171-194.

Mansell, E. R., 2010: On sedimentation and advection in multimoment bulk microphysics. *J. Atmos. Sci.*, **67**, 3084–3094, doi: 10.1175/2010JAS3341.1.

Mitzeva, R. P., J. Latham, and S. Petrova, 2006: A comparative modeling study of the early electrical development of maritime and continental thunderstorms. *Atmos. Res.*, **82**, 26–36, doi: 10.1016/j.atmosres.2005.01.006.

Saunders, C. P. R. and S. L. Peck, 1998: Laboratory studies of the influence of the rime accretion rate on charge transfer during crystal/graupel collisions. *J. Geophys. Res.*, **103**, 13949–13956.

Shu, C.-W., 2003: High-order finite difference and finite volume WENO schemes and discontinuous Galerkin methods for CFD. Int. J. Comp. Fluid Dyn., 17, 107–118.

Takahashi, T., 1984: Thunderstorm electrification – a numerical study. *J. Atmos. Sci.*, **41**, 2541–2558.

Tremback, C. J., J. Powell, W. R. Cotton, and R. A. Pielke, Sr., 1987: The forward-in-time upstream advection scheme: Extension to higher orders. *Mon. Wea. Rev.*, **115**, 540–555.

Wicker, L. J. and W. C. Skamarock, 2002: Time-splitting methods for elastic models using forward time schemes. Mon. Wea. Rev., 130, 2088–2097.

Wicker, L. J. and R. B. Wilhelmson, 1995: Simulation and analaysis of tornado development and decay within a three-dimensional supercell thunderstorm. J. Atmos. Sci., 52, 2675– 2703.

Ziegler, C. L., 1985: Retrieval of thermal and microphysical variables in observed convective storms. Part I: Model development and preliminary testing. J. Atmos. Sci., 42, 1487–1509.

Ziegler, C. L., D. R. MacGorman, J. E. Dye, and P. S. Ray, 1991: A model evaluation of non-inductive graupel-ice charging in the early electrification of a mountain thunderstorm. *J. Geophys. Res.*, **96**, 12833–12855.

Ziegler, C. L., T. J. Lee, and Roger A. Pielke, Sr., 1997: Convective initiation at the dryline: A modeling study. Mon. Wea. Rev., 125, 1001–1026.